

DesignEdit: Multi-Layered Latent Decomposition and Fusion for Unified & Accurate Image Editing

Yueru Jia¹ Yuhui Yuan^{1,2,3} Aosong Cheng Chuke Wang Ji Li Huizhu Jia Shanghang Zhang³

¹joint core contribution ²project lead ³corresponding author

Microsoft Research Asia Peking University

<https://design-edit.github.io/>

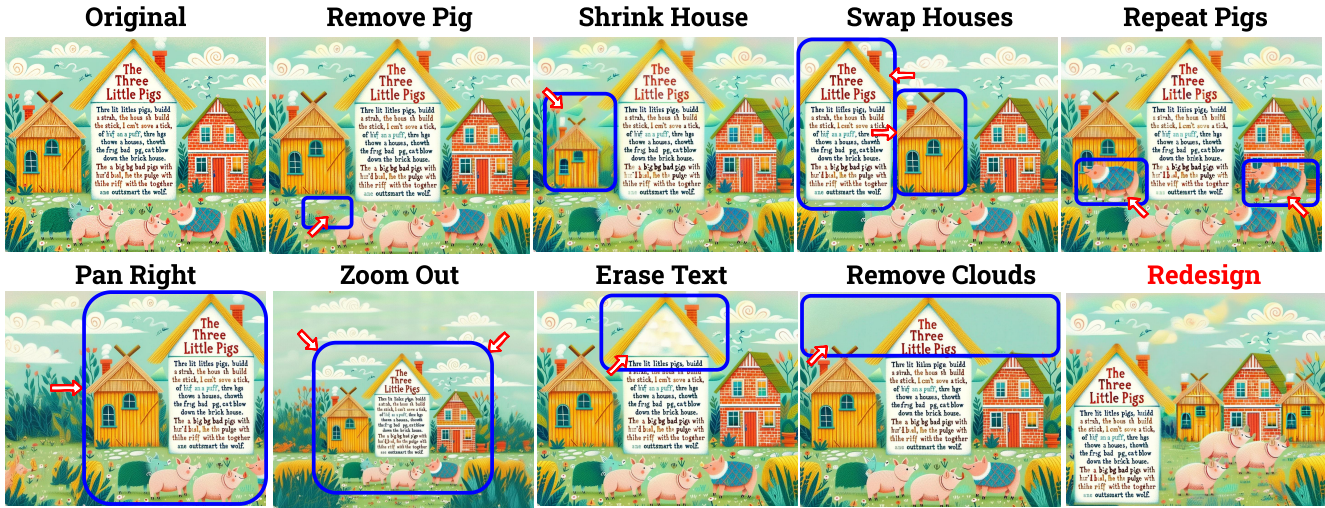


Figure 1. **Examples of visual design image editing.** Our approach facilitates a range of image editing operations with a training-free and unified framework to achieve accurate spatial-aware editing of the design image. Our approach is able to manipulate different objects simultaneously, as well as implement various operations at the same time. All results are produced using one diffusion denoising process.

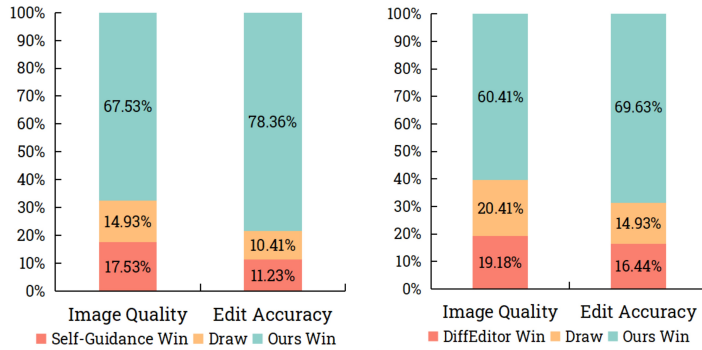
Abstract

Recently, how to achieve precise image editing has attracted increasing attention, especially given the remarkable success of text-to-image generation models. To unify various spatial-aware image editing abilities into one framework, we adopt the concept of layers from the design domain to manipulate objects flexibly with various operations. The key insight is to transform the spatial-aware image editing task into a combination of two sub-tasks: multi-layered latent decomposition and multi-layered latent fusion. First, we segment the latent representations of the source images into multiple layers, which include several object layers and one incomplete background layer that necessitates reliable inpainting. To avoid extra tuning, we further explore the inner inpainting ability within the self-attention mechanism. We introduce a key-masking self-attention scheme that can propagate the surrounding context information into the masked region while mitigat-

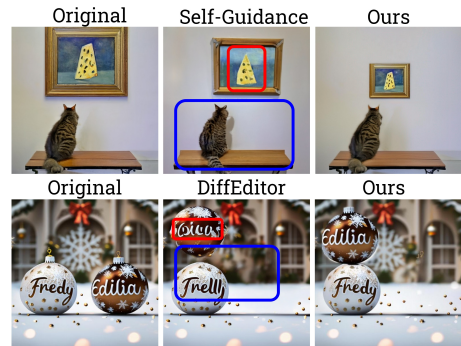
ing its impact on the regions outside the mask. Second, we propose an instruction-guided latent fusion that pastes the multi-layered latent representations onto a canvas latent. We also introduce an artifact suppression scheme in the latent space to enhance the inpainting quality. Due to the inherent modular advantages of such multi-layered representations, we can achieve accurate image editing, and we demonstrate that our approach consistently surpasses the latest spatial editing methods, including Self-Guidance and DiffEditor. Last, we show that our approach is a unified framework that supports various accurate image editing tasks on more than six different editing tasks.

1. Introduction

Despite the great achievements in image generation by training large-scale text-to-image diffusion models [10, 15, 18, 23, 26, 27], as demonstrated by recent seminal research



(a) Win rates comparison in image quality and edit accuracy



(b) Visual comparison of single-object editing

Figure 2. Comparison between our method against Self-Guidance and DiffEditor. We report the win-rate comparison across image quality and edit accuracy in (a). For each comparison, we select 10 examples with multiple operations like movement and resizing. Users were asked to vote from two aspects, image quality and edit accuracy. The “Draw” option represents equal effect. We collect answers from 73 users, with a total of 1460 votes for each metric.

including SDXL [21], DALL-E3 [3, 19] and Ideogram¹, these models face challenges with prompts requiring numeracy or spatial arrangement capability, for example, Figure 1 (a) showcases a captivating storybook design image generated by DALL-E3 with the text prompt describing the story of the “three pigs”. We find there are four pigs in the figure, which is not consistent with “three pigs” in the text prompt. To overcome these limitations, cutting-edge efforts [9, 16, 17, 28] have been directed towards developing precise spatial-aware image editing techniques, aiming to bridge the discrepancy between user expectations and initial generation outcomes.

Unlike previous methods [9, 16, 17, 28] that require combining multiple editing guidance designs for different editing tasks and updating the latent representations through additional backpropagation, we propose a training-free, forward-only, and unified framework for accurate spatial-aware image editing tasks. Our approach transforms most of the representative spatial-aware editing tasks into a two-fold process. This process involves first decomposing the multi-layered latent representations of source images based on precise user instructions and the layer segmentation masks, and then integrating these representations into target images in accordance with an accurate layout arrangement. To ensure accurate spatial-aware editing quality of multiple image layers, we explicitly fuse the multiple layered latents following the target layout arrangement to form the target latent representations. Additionally, we support leveraging the reasoning and visual planning capabilities of GPT-4V [34] to assist in crafting user instructions and generating (and refining) accurate layout arrangements.

We identify the key challenges in performing the multi-

layered latent decomposition and fusion process, and then present three non-trivial technical contributions as follows:

(i) First, we observe that one of the key challenges in performing the multi-layered latent decomposition lies in generating a high-quality background layer. This layer should not only maintain faithfulness to the original ones but also inpaint the incomplete regions of the decomposed object layers. Instead of applying existing inpainting methods, we introduce a very simple yet more reliable self-attention [31] key-masking approach that consistently achieves much better inpainting quality. (ii) Second, another challenge we need to address is that the inpainted region might suffer from the negative influence of some unrelated areas, leading to artifacts. Therefore, we propose an artifact suppression scheme to further enhance the inpainting quality. (iii) Third, we introduce a unified framework for various image editing tasks by breaking them down into two fundamental sub-tasks: multi-layered latent decomposition and multi-layered latent fusion.

We perform an extensive user study to evaluate the image editing quality of our approach, comparing it to the latest advancements in Self-Guidance [9] and DiffEditor [17]. The outcomes, illustrated in Figure 2, showcase the win rates across two key dimensions: image quality and editing fidelity. Our findings demonstrate that our method significantly outperforms these two benchmark approaches in various editing tasks, such as object movement and resizing. Additionally, we apply our approach to a range of challenging design image editing tasks, such as object removal, resizing, movement, repetition, flipping, camera panning, zooming out, composing multiple images, and editing typography or decorations, among others. We hope to inspire further developments in more precise spatial-aware image editing technologies.

¹<https://ideogram.ai/>

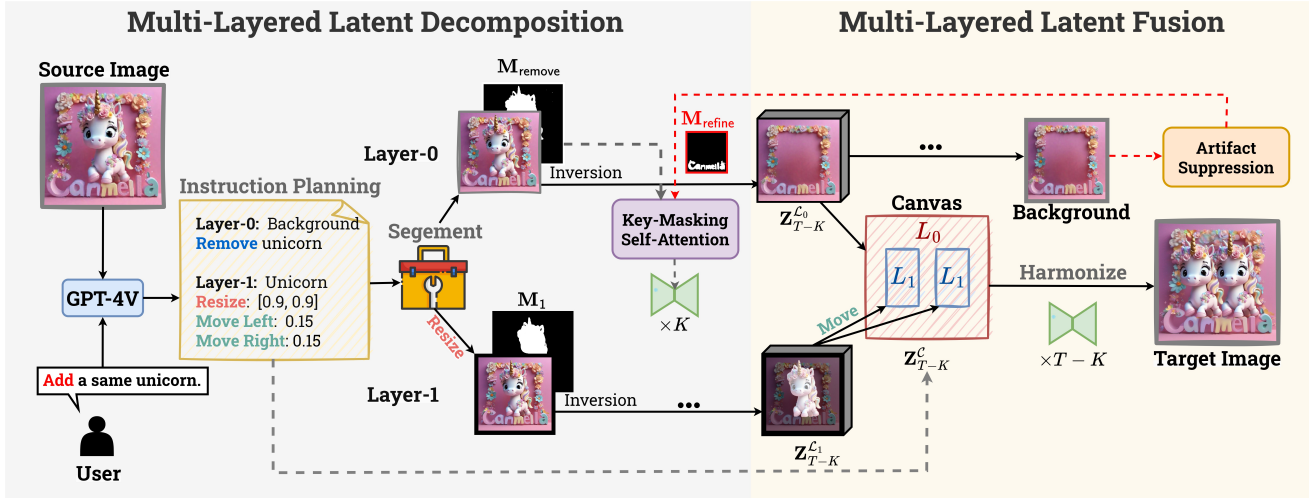


Figure 3. **Illustrating the overall framework of our approach:** During the multi-layered decomposition stage, given a user’s editing instruction and the source image, we first utilize GPT-4V to perform instruction planning, generating a set of detailed layer-wise editing instructions. Then, we segment the source image into multiple image layers, including the background layer that requires additional inpainting, implemented by a novel key-masking self-attention scheme, and the other object layers of the object to manipulate. For the multi-layered fusion stage, We follow the layers’ orders and layer-wise instructions sequentially to paste them onto the canvas in latent space. We further apply multiple denoising steps to harmonize the fused multi-layered latent representations. Additionally, we perform artifact suppression to improve the background inpainting quality.

2. Related Work

2.1. Latent Diffusion Model

Latent Diffusion Models [24] (LDMs) introduce a groundbreaking approach to the field of generative modeling by operating in a compressed latent space, rather than at the image level. This method accelerates the generation process and reduces computational demands. Recently, large-scale conditional diffusion models [21, 24, 27] that adopt the architecture of latent diffusion models and are trained on a large amount of data, can generate images that are both rich in detail and visually appealing. Image editing methods like Blended Latent Diffusion [2] demonstrate that operating in the latent space can achieve local image adjustments with faster inference and better precision than operating at the image level [1]. In our work, we adopt the state-of-the-art large-scale text-to-image LDMs, Stable Diffusion [21, 24] with U-Net structure [25], to further explore latent operations for spatial-aware image editing.

2.2. Guidance-Driven Spatial-aware Image Editing

Spatial editing involves modifying images by considering the spatial context and relationships within the image. This includes removing, moving, resizing, or adding elements, in contrast to in-place editing methods [4, 5, 12, 13].

Inspired by the classifier guidance strategy on diffusion models, Training-free Layout Control [7] and Boxdiff [32] constrain the latent space using position information loss to achieve spatial-aware image generation with layout con-

trol. Self-Guidance [9] introduces classifier-guidance into diffusion-based image editing to complete tasks like object movement and resizing. DragonDiffusion [16], inspired by DragGAN [20], incorporate dragging-based image editing tasks into diffusion models, extending to more spatial-aware editing tasks, such as object movement and resizing with image prompts like object masks. DiffEditor [17] improves DragonDiffusion to achieve state-of-the-art results in accurate image editing tasks.

These guidance-driven methods [6, 9, 16, 17, 35, 39] rely on loss backward, leading to the entanglement among various elements, making it impractical to perform different operations on different objects simultaneously. Ours solves the problem by multi-layer decomposition, utilizing the flexibility of layers to achieve more complex and general editing tasks. On the other hand, loss is a soft constraint that ignores or modifies relative pixel-level features, potentially leading to changes in object and background identity. Our multi-layer fusion strategy directly follows layer-wise editing instructions in latent space. Additionally, our approach facilitates object removal with performance matching that of specifically trained or tuned inpainting models, a capability lacking in guidance-driven methods.

3. Approach

The key idea of our work is at presenting a training-free multi-layered decomposition and fusion framework that can unify various spatial-aware image editing tasks. First, we ex-

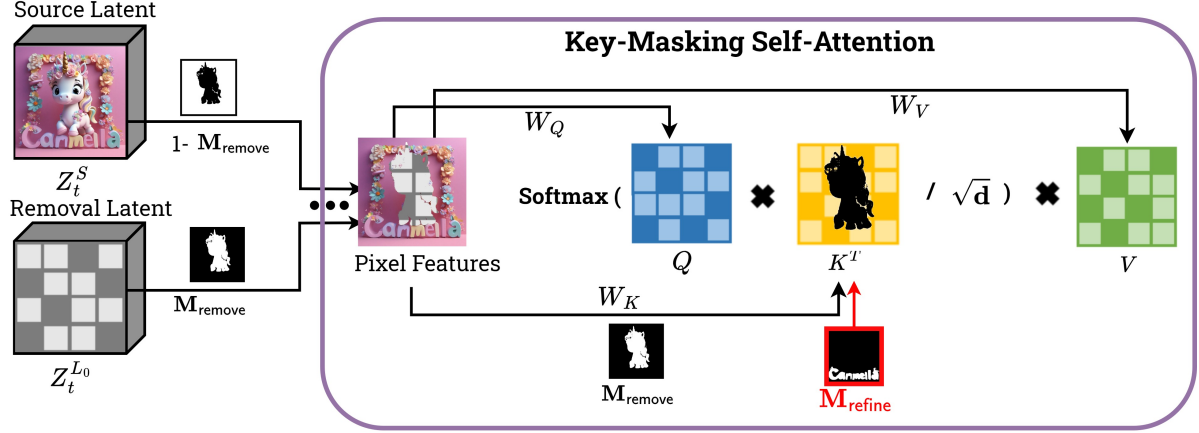


Figure 4. **Key-Masking Self-Attention Mechanism at time step t .** The figure shows the diagram for the removal latent Z_t^S at timestep t . The surroundings of pixel features are kept by the source latent Z_t^S . M_{remove} and M_{refine} are utilized on key features to reduce attention within the mask.

plain the detailed design of multi-layered latent decomposition stage that prepares the precise layered-latent representations associated with different objects based on a set of object segmentation masks. Additionally, we leverage the reasoning and planning capabilities of GPT-4V to automatically transform user editing requests into structured, layer-wise editing instructions by providing several in-context examples. Second, we demonstrate a multi-layered latent fusion scheme that integrates multiple latent representations in accordance with a target layout canvas, which can be supplied by either human input or GPT-4V. Last, we enhance the harmony of the fused target latent representations by applying additional diffusion steps. Moreover, we introduce an artifact suppression refinement strategy to check and enhance the effectiveness of the background removal. Figure 3 illustrates the overall pipeline of our approach.

3.1. Multi-Layered Latent Decomposition

Inspired by the concept of layers in the design domain, we introduce a multi-layered latent decomposition scheme to simplify the complex image editing process into a set of independent, easily manageable layer-wise editing operations for each image layer. In this study, we conceptualize a “layer” as either a singular basic visual element or a collection of multiple visual elements within the source image. Each layer can be independently adjusted, removed, or merged with others, facilitating precise manipulation of the final image composition.

Given a source image and an editing instruction, we need to perform layer-wise editing instruction planning and prepare the multi-layered latent representations. More details are illustrated as follows.

Layer-wise Editing Instruction Planning The key idea of this step is to leverage the reasoning and planning capabilities

of GPT-4V to transform vague user editing instructions into detailed and clear, layer-wise editing instructions. We support two types of spatial editing instructions: “Resize”, which adjusts size using height and width ratios, and “Move”, which adjusts position using direction and scale. The layer order depends on the sequence of pasting on the canvas. Layer-0 serves as the background layer, while Layer-1 to Layer-N serve as instance layers.

Layer-wise Mask Segmentation and Adjustment After generating the layer-wise editing instructions, we proceed with layer-wise mask segmentation for two purposes: object removal through the key-masking self-attention scheme and as foundational elements for constructing the layout canvas. An interesting observation we’ve made is that merely resizing the layer-wise latents can lead to blurring and artifacts. To address this, we resize both the initial image and mask, then encode the resized one into latent space while maintaining the object’s central positioning unchanged.

Key-Masking Self-Attention Then we encode the prepared layer image into latent space by inversion technique [11]. We introduce a novel key-Masking self-attention scheme within the U-Net structure of the Latent Diffusion Model to remove the regions inside the mask of Layer-0 and maintain the overall harmony of the background.

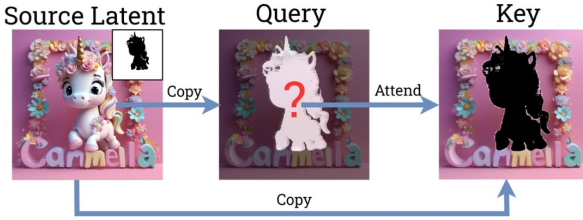
Key-Masking Self-Attention applies the removal mask M_{remove} to the KEY features of the self-attention during the initial K diffusion steps. The computational process is described as follows:

$$\text{Softmax} \left(\frac{\mathbf{Q} \left((1 - M_{remove}) \odot \mathbf{K} \right)^T}{\sqrt{d}} \right) \mathbf{V}, \quad (1)$$

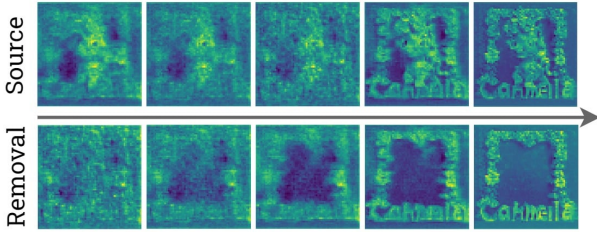
where Q, K, V come from the removal latent features $Z_T^{L_0}$, projected by W_Q, W_K, W_V .

To preserve the areas outside the mask, we replicate the surrounding features from the source latent \mathbf{Z}_t^S provided by the inversion path. $\mathbf{Z}_T^{\mathcal{L}_0}$ is initialized by \mathbf{Z}_T^S . As shown in Figure 4, at each denoising timestep t , we update the removal latent $\mathbf{Z}_t^{\mathcal{L}_0}$ to retain the latest surrounding features:

$$\mathbf{Z}_t^{\mathcal{L}_0} = \mathbf{Z}_t^{\mathcal{L}_0} \odot \mathbf{M}_{\text{remove}} + \mathbf{Z}_t^S \odot (1 - \mathbf{M}_{\text{remove}}). \quad (2)$$



(a) Illustration of the removal ability



(b) Visualization of the output from self-attention for the source and removal branches

Figure 5. **Illustrating the Key-Masking Self-Attention Mechanism.** (a) shows that regions inside the mask query only from the regions outside the mask, which are copied from the source latent to complete the information. (b) presents the output heatmaps changing over time from the source and removal latent. The maps come from the first self-attention block at a resolution of 64×64 .

Since attention weights are calculated by matching query and key, if a key is masked, the match degree of any query with this key will be very low. This results in the key’s corresponding regions $\mathbf{M}_{\text{remove}}$ not being considered in the weighted sum computation. Figure 5 (a) illustrates that by applying the mask to the key features, we enable the query to *ignore* the regions inside the mask, focusing only on the remaining areas. The regions inside the mask are reconstructed by consulting the remaining areas which are preserved step by step by \mathbf{Z}_t^S . Figure 5 (b) visualizes heatmaps of the output features of self-attention from the source latent \mathbf{Z}_t^S and the removal latent $\mathbf{Z}_t^{\mathcal{L}_0}$. We observe that information corresponding to the masked region is suppressed in the final output, receiving a lower attention score compared to the source latent, while ensuring a gradual transition with the surrounding background.

3.2. Multi-Layered Latent Fusion

Instruction-Guided Latent Fusion After the first K steps of removal on the background layer L_0 , we sequentially paste the prepared layered latent features onto the layout canvas latent \mathbf{Z}_t^C at timestep $T - K$ with layer-wise “Move” instructions V_i .

Given a two-dimensional operating vector $\mathbf{v} = (dx, dy)$, we define the operation $\text{Move}(I; \mathbf{v}) : B \times C \times H \times W \rightarrow B \times C \times H \times W$ as follows:

$$I'(i, j) = \text{Move}(I; \mathbf{v})(i, j) = I(i - dx, j - dy),$$

where B is the batch size, C is the channel numbers, and H and W are the image height and width, respectively. The operation moves the latent features and mask in a specific direction and scales them to achieve object movement.

At timestep $t = T - K$, first initialize layout canvas latent \mathbf{Z}_t^C with $\mathbf{Z}_t^{\mathcal{L}_0}$, and then for each Layer $L_i, i = 1, 2, \dots, N$ and for each operating vector $\mathbf{v}_j \in V_i$, we denote $\hat{\mathbf{M}}_i = \text{Move}(\mathbf{M}_i; \mathbf{v}_j)$, and the latent fusion process is described by the following equation:

$$\mathbf{Z}_t^C = \mathbf{Z}_t^C \odot (1 - \hat{\mathbf{M}}_i) + \text{Move}(\mathbf{Z}_t^{\mathcal{L}_i}; \mathbf{v}_j) \odot \hat{\mathbf{M}}_i. \quad (3)$$

Fused Latent Harmonization To enhance edge integration between layers and address abrupt changes at interfaces, we conduct a harmonization process after sequential layering, at the final $T - K$ denoising steps of the diffusion process. This method refines blending and reduces visual discrepancies at layer boundaries, improving image quality and realism.

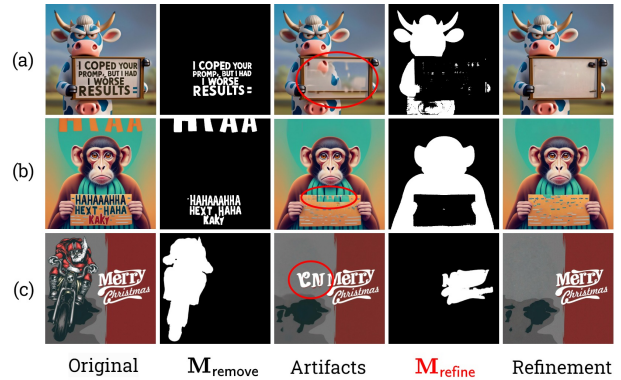


Figure 6. **Qualitative illustrations of the usage of $\mathbf{M}_{\text{refine}}$ in artifact suppression refinement.** (a) and (b) show text removal within board elements, while (c) shows the removal of regions near styled text.

Artifact Suppression Refinement By decoding the inpainted background image, we can check the removal results. For examples, as shown in Figure 6 (a) and (b), board

Editing Task	Adjust Image	Remove Mask M_{remove}	Source, Removal, Target	Fusion t
Object Removal	None	$\sum M_{\text{obj}}$	$Z_t^S, Z_t^{\mathcal{L}_0}, Z_t^{\mathcal{L}_0}$	None
Object Movement	None	$\sum M_{\text{obj}}$	$Z_t^S, Z_t^{\mathcal{L}_0}, Z_t^C$	$T - K$
Object Resizing, Flipping	Resize, Flip	$\sum M_{\text{obj}}$	$Z_t^S, Z_t^{\mathcal{L}_0}, Z_t^C$	$T - K$
Camera Panning	Pan and Paste	M_{pan}	$Z_t^S, Z_t^{\mathcal{L}_0}, Z_t^{\mathcal{L}_0}$	None
Zooming Out	Zoom and Paste	M_{zoom}	$Z_t^S, Z_t^{\mathcal{L}_0}, Z_t^{\mathcal{L}_0}$	None
Occlusion-Aware Editing	None	$\sum_{v_j \in V_i} \text{Move}(M_{\text{occlude}}; \mathbf{v}_j)$	$Z_t^C, \hat{Z}_t^C, \hat{Z}_t^C$	$T - K \sim 0$
Cross-Image Composition	Layout-guided	M_{BG}	$Z_t^{\text{BG}}, Z_t^{\mathcal{L}_0}, Z_t^C$	$T - K$

Table 1. **Unified Overview of Spatial-Aware Image Editing Tasks.** ‘‘Source’’ represents the initial latent before removal, as defined in Equation (1) and (2). ‘‘Removal’’ refers to the latent to apply key-masking self-attention in Equations (1) and (2). ‘‘Target’’ latent is used to decode the final output. ‘‘Fusion step t ’’ is the range where Equation (3) is implemented.

elements are common in design images, and removing too much content from the board may result in missing parts.

It’s also difficult for the diffusion model to recognize styled typography in some cases, so it tends to extend them in the removal area, as shown in Figure 6 (c).

To address this issue, we introduce a refinement process, Artifact Suppression. The central idea is to guide the model to avoid focusing on the parts that cause artifacts, which are identified by M_{refine} . M_{refine} is applied together with M_{remove} in the Key-Masking Self-Attention Mechanism; it does not affect the latent operations in Equation (1). This refinement process enables us to achieve a high success rate in removing content from the source image. The modified key-masking self-attention mechanism is:

$$\text{Softmax} \left(\frac{\mathbf{Q} \left((1 - M_{\text{remove}} - M_{\text{refine}}) \odot \mathbf{K} \right)^T}{\sqrt{d}} \right) \mathbf{V}. \quad (4)$$

3.3. Unifying Spatial-aware Image Editing Tasks

Sections 3.1 and 3.2 present a general framework for multi-layered representation in image editing. With this framework, we can unify various basic spatial-aware editing operations along with their extensions in Table 1: The removal of masked regions from the ‘‘Source’’ latent is achieved by applying Key-Masking Self-Attention to the ‘‘Removal’’ latent, as described in Equation (1) and (2), thereby enabling multi-layered decomposition. Multi-layered latent fusion is executed by applying Equation (3) to the ‘‘Canvas’’ latent Z_t^C .

Object Removal, Movement, Resizing and Flipping These are basic editing operations. Resizing and flipping require an additional layer for image-level adjustments to the source image before encoding. Movement is executed during the fusion stage. The M_{remove} is the union of masks for all objects needing manipulation, denoted as $\sum M_{\text{obj}}$.

Camera Panning and Zooming Out By adjust the initial image and generating two specific masks, we can convert the tasks of camera panning and zooming out into a removal task. We pan or zoom the source image and paste it onto the original canvas to initialize the removal regions with its adjacent areas, ensuring smooth transitions and color consistency. As shown in Figure 7, regions corresponding to the original image are set to 0, and the remaining regions needing completion are set to 1. At the $T \sim$

$T - K$ Removal Stage in Equations (1) and (2), we simply replace the M_{remove} with $M_{\text{pan/zoom}}$.

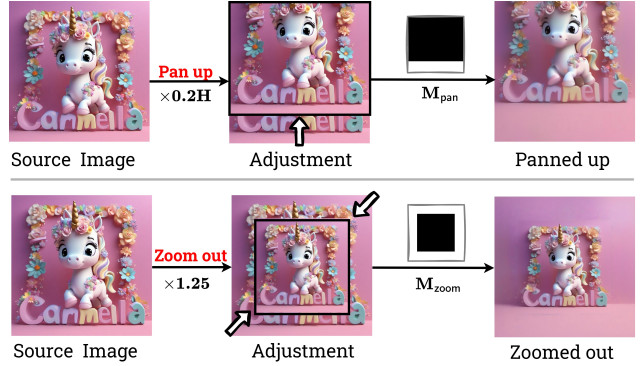


Figure 7. **Illustration of the mask usage in camera panning and zooming out tasks.** The figure presents two cases of image adjustment and the formation of their related masks.

Occlusion-Aware Object Editing Note that objects often do not appear completely in the source image. For example in Figure 8, one of the dog’s legs is occluded by the ball. Direct relocation results in incomplete failure. We present a novel strategy called *Integrated Decomposition-Fusion Technique*, making full use of the inpainting ability of the Key-Masking Self-Attention.

The illustration pipeline is shown in Figure 8. For every iteration of the first K diffusion steps, besides the background removal on $Z_t^{\mathcal{L}_0}$, we first perform the fusion operation on the canvas latent with Equation (3), and then we introduce a new mask M_{occlude} , which in this example is the initial ball mask. In this case, the removal latent is represented by the canvas latent \hat{Z}_t^C , which is guided by the source latent Z_t^C :

$$\hat{Z}_t^C = \hat{Z}_t^C \odot \hat{M}_{\text{occlude}} + Z_t^C \odot (1 - \hat{M}_{\text{occlude}}). \quad (5)$$

We denote $\hat{M}_{\text{occlude}} = \sum_{v_j \in V_i} \text{Move}(M_{\text{occlude}}; \mathbf{v}_j)$ to represent the sum of masks after moving with the occluded Layer- i L_i . The Key-Masking Mechanism is to replace M_{occlude} with M_{remove} in Equation (1) on canvas latent \hat{Z}_t^C . Integrated Decomposition-Fusion Technique is a more general fusion strategy and in non-occluded image editing contexts, it equals the one-step fusion at $t = T - K$, and the latter has a lower computational cost.

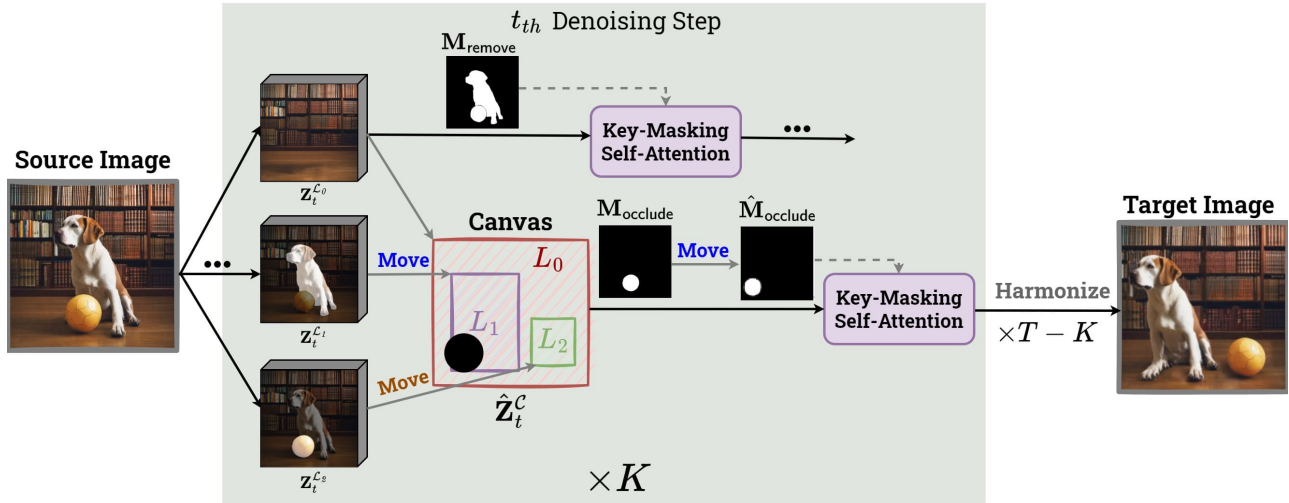


Figure 8. **Illustrating the Integrated Decomposition-Fusion Technique in occlusion-aware object editing at timestep t .** To relocate the dog and ball and inpaint the occluded dog leg, we conduct Key-Masking Self-Attention twice on the background latent $\mathbf{Z}_t^{\mathcal{L}_0}$ and the canvas latent $\mathbf{Z}_t^{\mathcal{L}_1}$ respectively. $\hat{\mathbf{M}}_{\text{occlude}}$ represents the moved $\mathbf{M}_{\text{occlude}}$ with the occluded Layer-1 $\mathbf{Z}_t^{\mathcal{L}_1}$. The target latent is the new canvas removal latent $\hat{\mathbf{Z}}_t^{\mathcal{C}}$.

Methods	L1↓	L2↓	CLIP-I↑	DINO↑	CLIP-T↑	FID↓	LPIPS↓	train or finetune	base model
Lama	0.014	0.004	0.985	0.979	0.307	25.077	0.053	✓	-
ControlNet-inpainting	0.025	0.010	0.951	0.905	0.300	59.322	0.095	✓	SD-v1.5
SDXL-inpainting	0.030	0.005	0.968	0.959	0.303	44.621	0.069	✓	SDXL-1.0
Uni-paint	0.064	0.020	0.920	0.837	0.298	103.846	0.156	✓	SD-v1.4
Ours	0.028	0.007	0.969	0.971	0.306	38.883	0.070	×	SDXL-1.0

Table 2. **Quantitative study on the MagicBrush test set for the mask-guided object removal task.** Bold, Red and Blue represent the top-3 results. Our method is the only one that does not require training or finetuning, and it achieves results comparable to SDXL-Inpainting across 7 metrics in 51 examples. Other methods are specifically trained or fine-tuned for mask-guided image inpainting.

Cross-Image Composition Our approach can support cross-image composition by encoding a background reference image (\mathbf{Z}_t^{BG}) and a set of foreground images. The layered instructions and order are given by the new layout design.

4. Experiment

Implementation Details We made structural modifications to SDXL-1.0 [21] using the frozen weights and generated images at a resolution of 1024×1024 . As a latent diffusion model, the resolution of SDXL-1.0’s latent space is 128×128 . We adopt the state-of-the-art diffusion inversion technique, Proximal-Guidance [11], to invert the source image into latent space and utilized a 50-step DDIM [29] denoising procedure, which means $T = 50$. We selected the most effective value for K , which is $K = 40$. The key-masking self-attention is applied across all 70 self-attention blocks in SDXL-1.0, with a range of $[50 \sim 10]$.

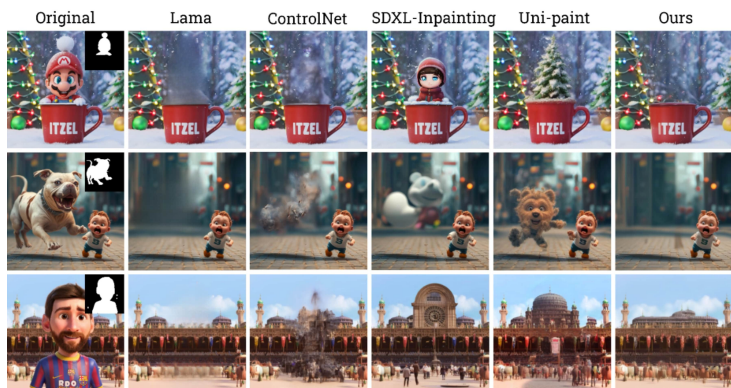
4.1. Comparison to State-of-the-art

Object Removal We compare the removal ability of our methods with other 5 methods specifically designed for inpainting

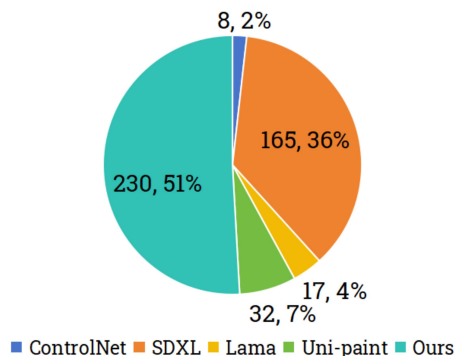
tasks: Lama [30], ControlNet-inpainting [37], SDXL-inpainting, and Uni-paint [33] on the MagicBrush benchmark [36]. In our experiments, we utilize data with instructions that are only about removal, with a total of 51 examples, each including a ground truth image generated by DALL·E 2 [23] for evaluation.

We evaluated the performance of our method and mask-guided image editing method on 7 metrics. L1 and L2 are used to gauge the pixel-level difference between the target image and the ground truth. CLIP-I [22] and DINO [8] are used to assess image quality, and CLIP-T is used to test text-image alignment. We also utilize the LPIPS [38] to measures perceptual differences at a patch level, and FID [14] to assess the similarity between the distributions of real and generated images’ features. The quantitative results in Figure 2 show the absolute strength of Lama, which is specifically trained for inpainting. Ours achieves results comparable to SDXL-Inpainting across 7 metrics but do not need any finetuning.

Users were asked to choose the best based on clarity, part restoration, and edge quality. We received 452 votes from 113 users, and the results are shown in Figure 9 (b), which demonstrates the superior performance of our method. Note that although LaMa performs best in benchmark tests, it produces noticeable



(a) Qualitative comparison results with inpainting models



(b) The vote count and percentage in user study

Figure 9. **Comparison with other mask-guided inpainting models.** (a) shows qualitative the comparison of large object removal ability, with our method not causing obvious blurriness or filling the removed area with unrelated elements. (b) shows the user study results of 452 votes from 113 users, with our method achieving a 51% preference percentage.

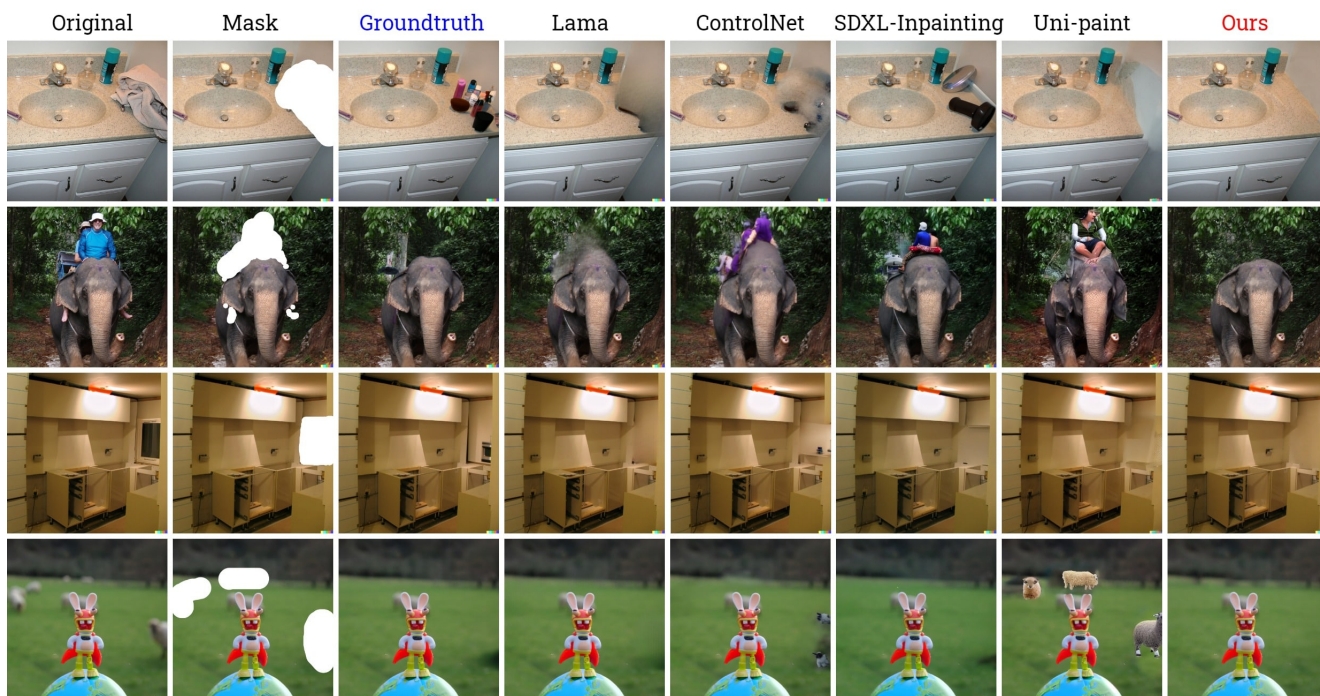


Figure 10. **Qualitative comparison on the MAGICBRUSH dataset.** We chose the mask-provided instruction-guided removal tasks to evaluate the inpainting ability of our method. The third column shows the removal results provided by DALL-E2 serving as ground truth. We compare the results of LaMa, ControlNet-Inpainting, SDXL-inpainting, Uni-paint with ours.

blurring artifacts when removing large areas, as shown in the second column of Figure 9 (a). This is why it received a low vote count in user studies.

Object Spatial-aware Editing We present further qualitative comparisons of single-object resizing and movement capabilities between Self-Guidance [9], DiffEditor [17], and our method in Figure 11. Our method demonstrates better inpainting perfor-

mance and superior editing accuracy in preserving the identity of the object and the background, especially with text and large objects. Note that for the other two methods, it is challenging to remove objects or edit two or more objects with different instructions in a single round, such as swapping.



Figure 11. **More qualitative comparisons with Self-Guidance and DiffEditor.** We conduct single-object editing tasks for movement (the first row) and resizing (the second row). The results in (a) come from the initial paper on Self-Guidance.

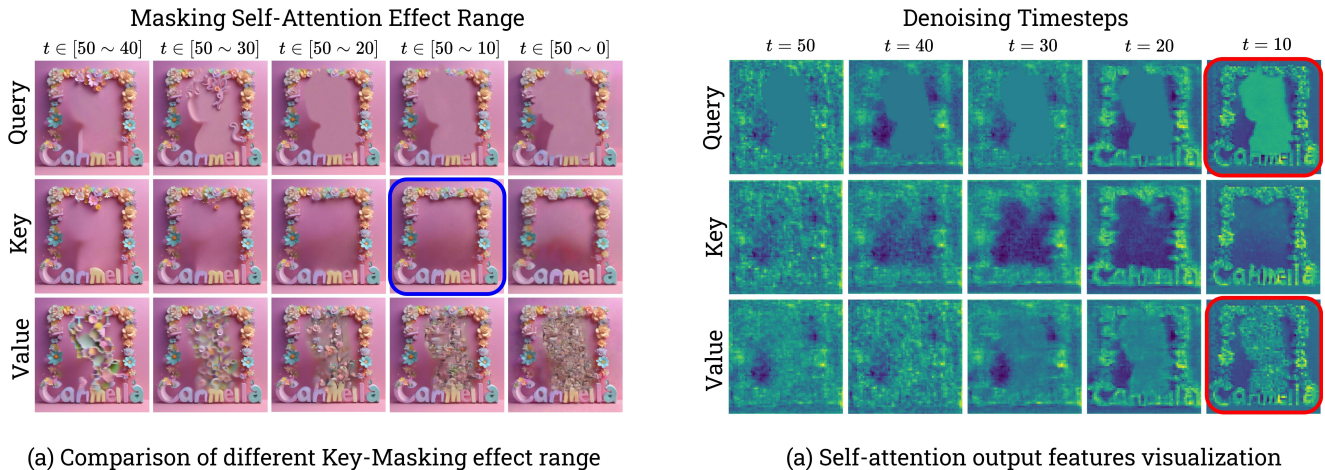


Figure 12. **The ablation study of different mask placements and effect range of self-attention.** (a) demonstrates the removal results under different masking effect ranges. (b) visualizes the self-attention output at different timesteps under the effect range $[50 \sim 10]$, same with the settings highlighted blue box in (a).

4.2. Ablation Study

Effect Range of Key-Masking Self-Attention By implementing Equation (2) across the entire range $[50 \sim 0]$ to maintain the surrounding features consistent with the source image, we investigate which effect range results in the most effective removal. As illustrated in the second row of Figure 12 (a), significant removal can be achieved within the first 10 steps of key-masking, while the range $[50 \sim 10]$ more effectively integrates the edges and blends better with the background. Therefore, we use $K = 40$ as our optimal setting across all editing tasks.

Mask Positioning within Self-Attention Mechanisms We compare the results of different mask positioning for removal, as shown in Figure 12 (a). Masking the query tends to blur the removal area. As highlighted by the red boxes in Figure 12 (b), the significance of the masked area diminishes during the attention calculation, leading to a reduction in the clarity of the corresponding pixels. Applying masking to the value damages or disrupts the pixels within the masked area, as incorrect values are assigned to

these pixels, distorting the generated image. It is important to note that masking on the key results in a smooth transition in the self-attention output around the masked area, ensuring a more coherent integration with the surrounding information.

Layer-wise Size Adjustment: Latent vs. Image We adjust image size at the multi-layered decomposition stage, which is different from the position adjustment at the latent level. Here, we compare two resizing methods and use the zooming out task as an example, which can be considered as a global resizing of the original image. As shown in Figure 13 (a), the details of the girls’ faces are altered when resizing at the latent level (highlighted in blue circles) and tend to become blurry, losing detail, resulting in inconsistency between the original and target images, thus compromising accuracy.

There are two main reasons. First, the resolution difference: the resolution at the image level is 1024×1024 , whereas at the latent level, it is 128×128 . The resolution is much lower at the latent level, resulting in significantly lower information density. Second, information loss and compression: resizing in the latent

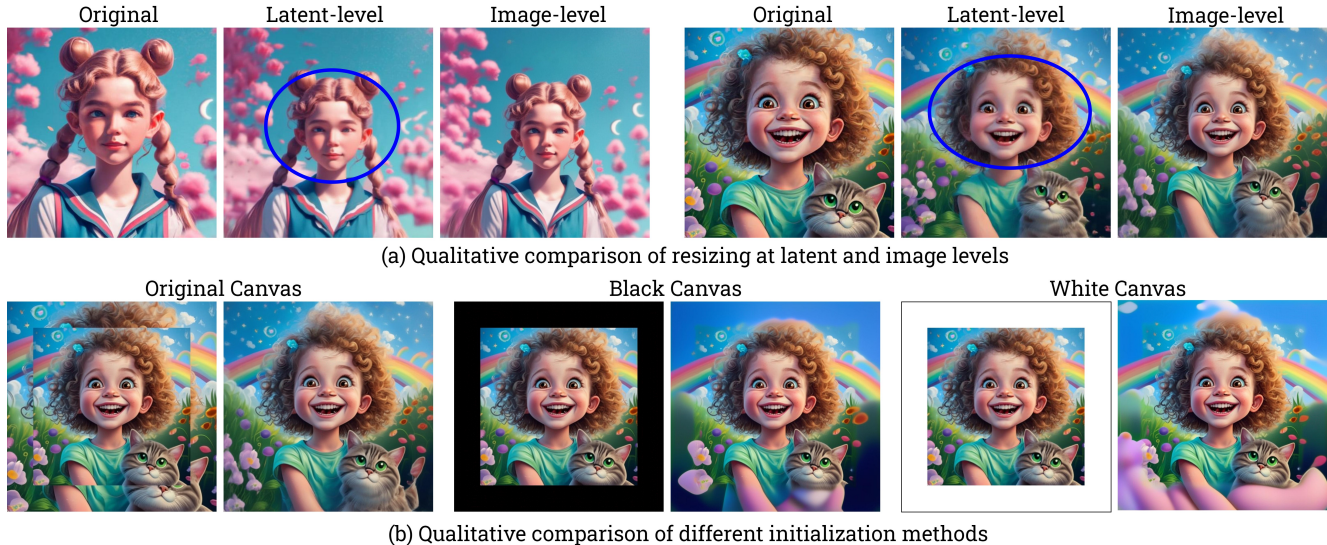


Figure 13. **The ablation study with zooming out task.** (a) illustrates the different resizing positions at the image level and latent level. (b) shows the different initialization methods with the original image, black canvas, and white canvas.

space essentially means further manipulating representations that have already been abstracted and compressed by the model. Due to the nonlinearity and complexity of this process, each feature point represents more abstract, higher-level information about the image.

Therefore, resizing at the latent level is more likely to result in the loss of these higher-level features, leading to a loss of detailed information. Due to the additional encoding and inversion costs associated with adjustments at the image level, we choose to perform position adjustments at the latent level, which has yielded satisfactory results.

Extra Canvas Initialization: Original Canvas vs. Black Canvas vs. White Canvas For camera panning and zooming out tasks, we first pan or zoom the initial image to the target position, and then paste it onto the initial image. This approach effectively initializes the regions within the mask using the surrounding areas. Initializing with the original canvas actually provides the model with clues and expected content to fill, allowing for the generation of details consistent with the surrounding environment. Additionally, the model attempts to maintain this coherence, producing content that matches the original image.

As demonstrated in Figure 13 (b), we explore two other initialization methods for the zooming out task: black canvas and white canvas. It’s observed that the first method inpaints the unknown areas with consistent, intricate details similar to the surroundings, effectively extending clouds, flowers, and the arm of the girl. However, the second and third methods result in inpainting regions that are disjointed and even discordant. This occurs because the model receives a “blank signal,” and relying solely on the self-attention mechanism’s queries makes it challenging to generate complex details closely connected to the original image.

4.3. More Qualitative Results

Multi-Object Complex Editing We demonstrate our multi-object editing ability with complex operations such as removal in Figure 14, swapping, relocation, resizing, addition, and flipping in Figure 15, and cross-image composition in Figure 16. All results are generated in one round.

Photorealistic Image Editing Section 4.1 and Figure 10 shows the removal ability on the photorealistic dataset MAGICBRUSH. Here we provide more qualitative results of different editing operations in Fig 17.

Applications on Design Images Figure 19 (b) illustrates the task of text-guided decoration removal with Cross-Attention masks, which are too irregular and numerous to mask manually. Figure 19 (b) and (c) show the applications in typography editing on design images with object removal and cross-image composition. Figure 18 shows poster editing results. Figure 20 shows the camera panning and zooming out results on design images.

5. Conclusion

In this study, we propose a multi-layered latent decomposition and fusion framework that unifies various spatial-aware image editing operations without requiring additional tuning. To enhance image editing precision, we introduce two innovative techniques: a key-masking self-attention scheme and an artifact suppression scheme, aimed at improving the quality of background image layers and occluded object layers. Additionally, we utilize the layout planning capability of the advanced GPT-4V models to further refine our approach. Finally, we empirically validate the superiority of our method across a range of image editing tasks, particularly in the challenging domain of design images, through comprehensive quantitative and qualitative comparisons.

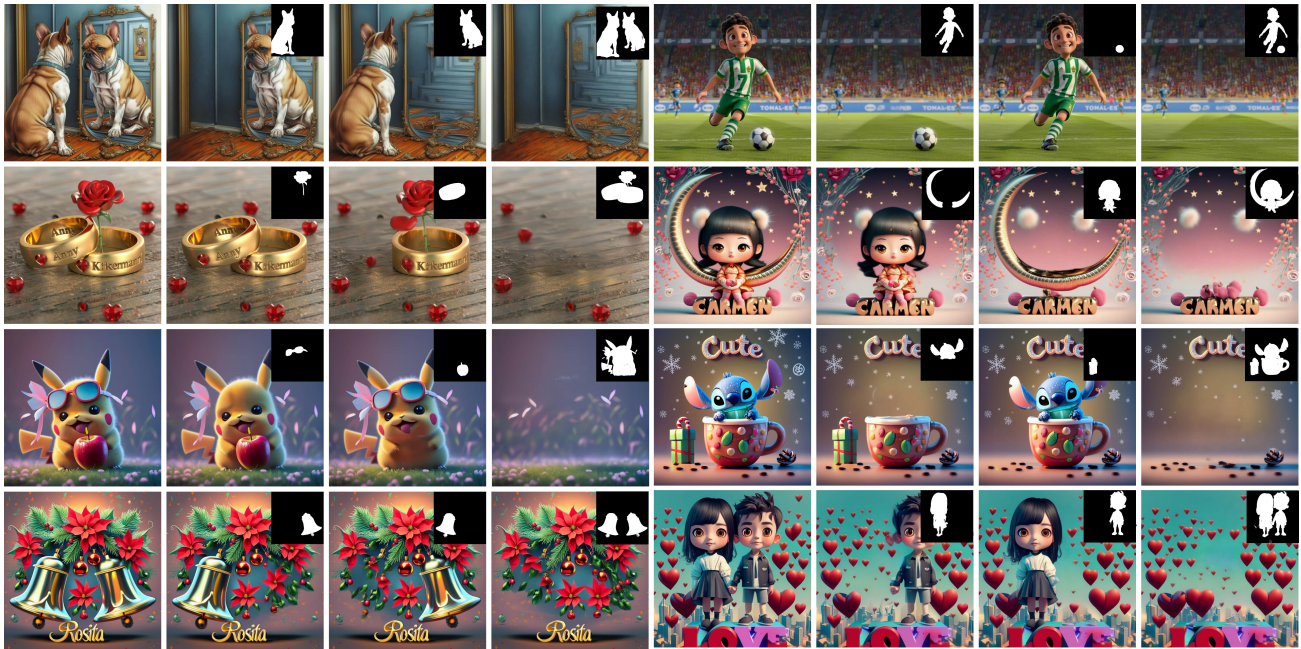


Figure 14. **Qualitative results of applications on design images.** The figure shows object removal results for single (the second and third columns) and multiple objects (the fourth column), covering the removal of both large and small areas.

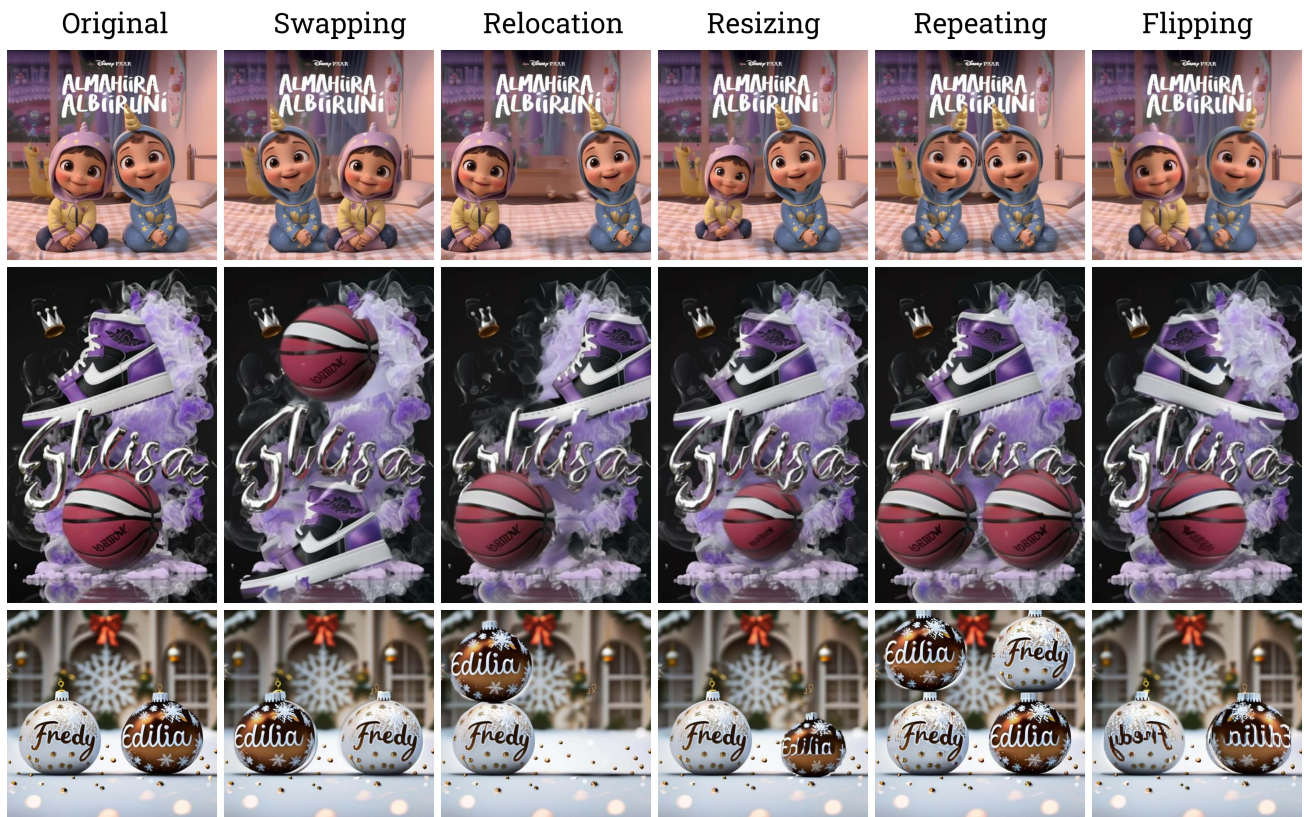


Figure 15. **Qualitative results of applications on design images.** The figure shows basic editing operations on two-object-centric design images with text elements.



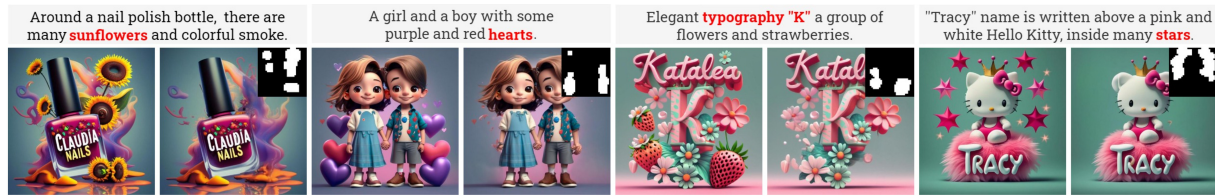
Figure 16. **Qualitative results of applications on design images.** The figure displays the background and foreground objects, along with their layer orders



Figure 17. **Qualitative results of photorealistic image editing.** We conduct basic editing operations to demonstrate our general editing ability, which is not limited to design images.



Figure 18. **Qualitative results of photorealistic image editing.** We show the results of removal and redesign on DALL-E3 posters in (a) and handmade posters in (b).



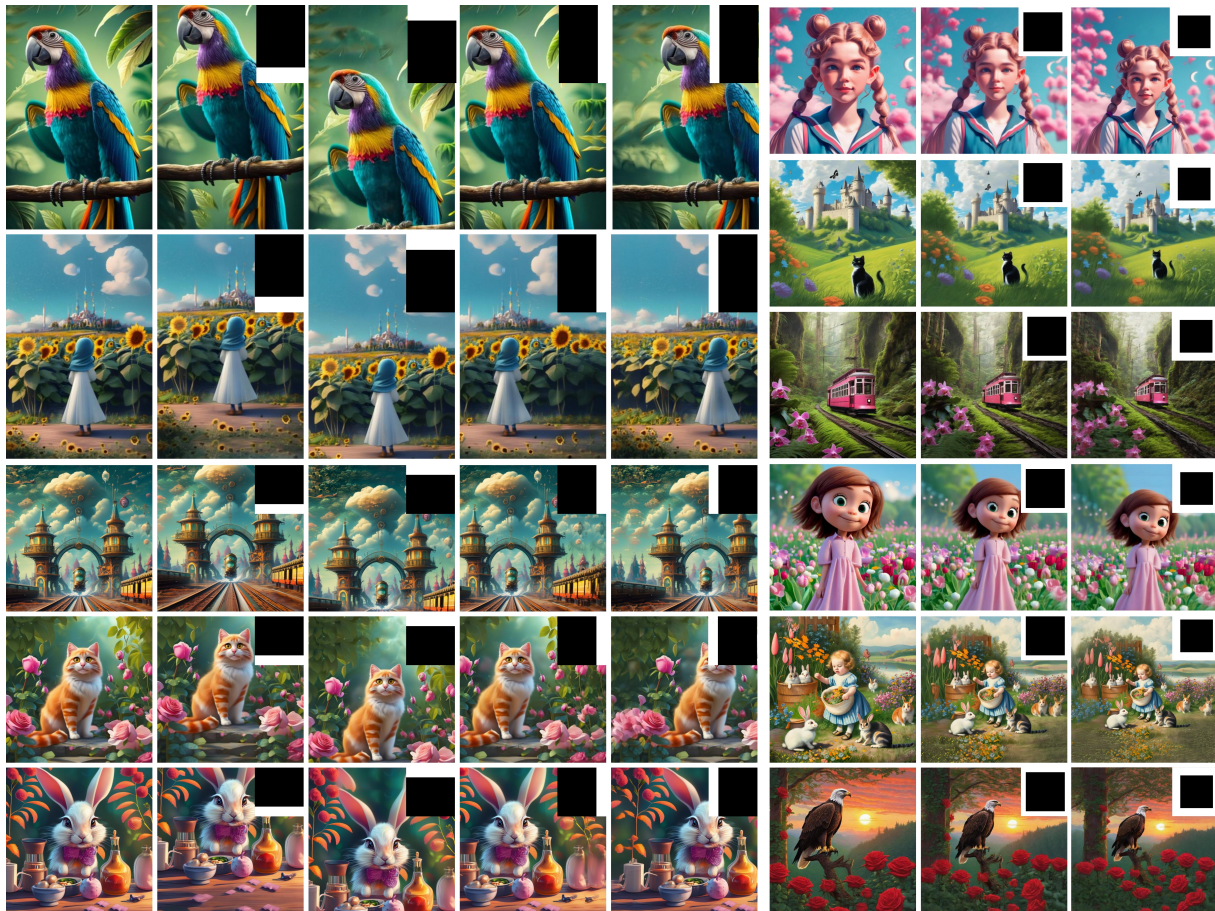
(a) Text-guided decoration removal



(b) Typography removal

(c) Typography retype with reference

Figure 19. **Qualitative results of applications on design images.** (a) shows the results of decoration removal using the Cross-Attention mask, with the relevant token marked in red. (b) and (c) demonstrate the results of typography editing.



(a) Camera panning

(b) Zooming out

Figure 20. **Qualitative results of camera panning and zooming out tasks.** (a) presents the qualitative results of camera panning in four directions: up, down, left, and right, with a scale of $0.2 \times H$ or $0.2 \times W$. (b) shows zooming out results at 1.25 and 1.5 scales.

References

- [1] Omri Avrahami, Dani Lischinski, and Ohad Fried. Blended diffusion for text-driven editing of natural images. In *2022 IEEE/CVF Conference on Computer Vision and Pattern Recognition (CVPR)*. IEEE, 2022. 3
- [2] Omri Avrahami, Ohad Fried, and Dani Lischinski. Blended latent diffusion. *ACM Transactions on Graphics (TOG)*, 42(4):1–11, 2023. 3
- [3] James Betker, Gabriel Goh, Li Jing, Tim Brooks, Jianfeng Wang, Linjie Li, Long Ouyang, Juntang Zhuang, Joyce Lee, Yufei Guo, Wesam Manassra, Prafulla Dhariwal, Casey Chu, Yunxin Jiao, and Aditya Ramesh. Improving image generation with better captions. Online, 2023. Accessed: 2024-01-03. 2
- [4] Tim Brooks, Aleksander Holynski, and Alexei A. Efros. Instructpix2pix: Learning to follow image editing instructions, 2023. 3
- [5] Mingdeng Cao, Xintao Wang, Zhongang Qi, Ying Shan, Xiaohu Qie, and Yinqiang Zheng. Masactrl: Tuning-free mutual self-attention control for consistent image synthesis and editing. *arXiv preprint arXiv:2304.08465*, 2023. 3
- [6] Hila Chefer, Yuval Alaluf, Yael Vinker, Lior Wolf, and Daniel Cohen-Or. Attend-and-excite: Attention-based semantic guidance for text-to-image diffusion models, 2023. 3
- [7] Minghao Chen, Iro Laina, and Andrea Vedaldi. Training-free layout control with cross-attention guidance. *arXiv preprint arXiv:2304.03373*, 2023. 3
- [8] Wenhui Chen, Hexiang Hu, Yandong Li, Nataniel Ruiz, Xuhui Jia, Ming-Wei Chang, and William W. Cohen. Subject-driven text-to-image generation via apprenticeship learning, 2023. 7
- [9] Dave Epstein, Allan Jabri, Ben Poole, Alexei A Efros, and Aleksander Holynski. Diffusion self-guidance for controllable image generation. *arXiv preprint arXiv:2306.00986*, 2023. 2, 3, 8
- [10] Shuyang Gu, Dong Chen, Jianmin Bao, Fang Wen, Bo Zhang, Dongdong Chen, Lu Yuan, and Baining Guo. Vector quantized diffusion model for text-to-image synthesis, 2022. 1
- [11] Ligong Han, Song Wen, Qi Chen, Zhixing Zhang, Kunpeng Song, Mengwei Ren, Ruijiang Gao, Yuxiao Chen, Di Liu 0003, Qilong Zhangli, et al. Improving tuning-free real image editing with proximal guidance. *CoRR*, 2023. 4, 7
- [12] Amir Hertz, Ron Mokady, Jay Tenenbaum, Kfir Aberman, Yael Pritch, and Daniel Cohen-Or. Prompt-to-prompt image editing with cross attention control, 2022. 3
- [13] Amir Hertz, Andrey Voynov, Shlomi Fruchter, and Daniel Cohen-Or. Style aligned image generation via shared attention, 2024. 3
- [14] Martin Heusel, Hubert Ramsauer, Thomas Unterthiner, Bernhard Nessler, and Sepp Hochreiter. Gans trained by a two time-scale update rule converge to a local nash equilibrium, 2018. 7
- [15] Bahjat Kawar, Shiran Zada, Oran Lang, Omer Tov, Huiwen Chang, Tali Dekel, Inbar Mosseri, and Michal Irani. Magic: Text-based real image editing with diffusion models. In *Proceedings of the IEEE/CVF Conference on Computer Vision and Pattern Recognition*, pages 6007–6017, 2023. 1
- [16] Chong Mou, Xintao Wang, Jiechong Song, Ying Shan, and Jian Zhang. Dragondiffusion: Enabling drag-style manipulation on diffusion models. *arXiv preprint arXiv:2307.02421*, 2023. 2, 3
- [17] Chong Mou, Xintao Wang, Jiechong Song, Ying Shan, and Jian Zhang. Diffeditor: Boosting accuracy and flexibility on diffusion-based image editing. *arXiv preprint arXiv:2402.02583*, 2024. 2, 3, 8
- [18] Alex Nichol, Prafulla Dhariwal, Aditya Ramesh, Pranav Shyam, Pamela Mishkin, Bob McGrew, Ilya Sutskever, and Mark Chen. Glide: Towards photorealistic image generation and editing with text-guided diffusion models, 2022. 1
- [19] OpenAI. DALL-E 3 System Card. Online, 2023. Accessed: 2024-01-03. 2
- [20] Xingang Pan, Ayush Tewari, Thomas Leimkühler, Lingjie Liu, Abhimitra Meka, and Christian Theobalt. Drag your gan: Interactive point-based manipulation on the generative image manifold. In *ACM SIGGRAPH 2023 Conference Proceedings*, pages 1–11, 2023. 3
- [21] Dustin Podell, Zion English, Kyle Lacey, Andreas Blattmann, Tim Dockhorn, Jonas Müller, Joe Penna, and Robin Rombach. Sdxl: Improving latent diffusion models for high-resolution image synthesis. *arXiv preprint arXiv:2307.01952*, 2023. 2, 3, 7
- [22] Alec Radford, Jong Wook Kim, Chris Hallacy, Aditya Ramesh, Gabriel Goh, Sandhini Agarwal, Girish Sastry, Amanda Askell, Pamela Mishkin, Jack Clark, Gretchen Krueger, and Ilya Sutskever. Learning transferable visual models from natural language supervision, 2021. 7
- [23] Aditya Ramesh, Prafulla Dhariwal, Alex Nichol, Casey Chu, and Mark Chen. Hierarchical text-conditional image generation with clip latents, 2022. 1, 7
- [24] Robin Rombach, Andreas Blattmann, Dominik Lorenz, Patrick Esser, and Björn Ommer. High-resolution image synthesis with latent diffusion models, 2022. 3
- [25] Olaf Ronneberger, Philipp Fischer, and Thomas Brox. U-net: Convolutional networks for biomedical image segmentation, 2015. 3
- [26] Nataniel Ruiz, Yuanzhen Li, Varun Jampani, Yael Pritch, Michael Rubinstein, and Kfir Aberman. Dreambooth: Fine tuning text-to-image diffusion models for subject-driven generation, 2023. 1
- [27] Chitwan Saharia, William Chan, Saurabh Saxena, Lala Li, Jay Whang, Emily L Denton, Kamyar Ghasemipour, Raphael Gontijo Lopes, Burcu Karagol Ayan, Tim Salimans, et al. Photorealistic text-to-image diffusion models with deep language understanding. *Advances in Neural Information Processing Systems*, 35:36479–36494, 2022. 1, 3
- [28] Yujun Shi, Chuhui Xue, Jiachun Pan, Wenqing Zhang, Vincent YF Tan, and Song Bai. Dragdiffusion: Harnessing diffusion models for interactive point-based image editing. *arXiv preprint arXiv:2306.14435*, 2023. 2
- [29] Jiaming Song, Chenlin Meng, and Stefano Ermon. Denoising diffusion implicit models. *arXiv preprint arXiv:2010.02502*, 2020. 7

- [30] Roman Suvorov, Elizaveta Logacheva, Anton Mashikhin, Anastasia Remizova, Arsenii Ashukha, Aleksei Silvestrov, Naejin Kong, Harshith Goka, Kiwoong Park, and Victor Lempitsky. Resolution-robust large mask inpainting with fourier convolutions. In *Proceedings of the IEEE/CVF winter conference on applications of computer vision*, pages 2149–2159, 2022. 7
- [31] Ashish Vaswani, Noam Shazeer, Niki Parmar, Jakob Uszkoreit, Llion Jones, Aidan N. Gomez, Lukasz Kaiser, and Illia Polosukhin. Attention is all you need, 2023. 2
- [32] Jinheng Xie, Yuexiang Li, Yawen Huang, Haozhe Liu, Wentian Zhang, Yefeng Zheng, and Mike Zheng Shou. Boxdiff: Text-to-image synthesis with training-free box-constrained diffusion. In *Proceedings of the IEEE/CVF International Conference on Computer Vision*, pages 7452–7461, 2023. 3
- [33] Shiyuan Yang, Xiaodong Chen, and Jing Liao. Uni-paint: A unified framework for multimodal image inpainting with pretrained diffusion model. In *Proceedings of the 31st ACM International Conference on Multimedia*. ACM, 2023. 7
- [34] Zhengyuan Yang, Linjie Li, Kevin Lin, Jianfeng Wang, Chung-Ching Lin, Zicheng Liu, and Lijuan Wang. The dawn of lmms: Preliminary explorations with gpt-4v(ision), 2023. 2
- [35] Jiwen Yu, Yinhuai Wang, Chen Zhao, Bernard Ghanem, and Jian Zhang. Freedom: Training-free energy-guided conditional diffusion model, 2023. 3
- [36] Kai Zhang, Lingbo Mo, Wenhui Chen, Huan Sun, and Yu Su. Magicbrush: A manually annotated dataset for instruction-guided image editing, 2023. 7
- [37] Lvmin Zhang, Anyi Rao, and Maneesh Agrawala. Adding conditional control to text-to-image diffusion models. In *Proceedings of the IEEE/CVF International Conference on Computer Vision*, pages 3836–3847, 2023. 7
- [38] Richard Zhang, Phillip Isola, Alexei A. Efros, Eli Shechtman, and Oliver Wang. The unreasonable effectiveness of deep features as a perceptual metric, 2018. 7
- [39] Min Zhao, Fan Bao, Chongxuan Li, and Jun Zhu. Egsde: Unpaired image-to-image translation via energy-guided stochastic differential equations, 2022. 3